Locating and quantifying CH_4 sources within a wastewater treatment plant based on mobile measurements

Junyue Yang[1], Zhengning Xu[1], Zheng Xia[4,5], Xiangyu Pei[1], Yunye Yang[1], Botian Qiu[2,3], Shuang Zhao[2,3], Yuzhong Zhang[2,3*], Zhibin Wang[1,6*]

[1]Zhejiang Provincial Key Laboratory of Organic Pollution Process and Control, MOE Key Laboratory of Environment Remediation and Ecological Health, College of Environmental and Resource Sciences, Zhejiang University, Hangzhou 310058, China

[2]Key Laboratory of Coastal Environment and Resources of Zhejiang Province, School of Engineering, Westlake University, Hangzhou 310030, China

[3]Institute of Advanced Technology, Westlake Institute for Advanced Study, Hangzhou 310024, China

[4]Ecological and Environmental Monitoring Center of Zhejiang Province, Hangzhou 310012, China

[5]Zhejiang Key Laboratory of modern Ecological and Environmental Monitoring, Hangzhou 310012, China

[6]ZJU-Hangzhou Global Scientific and Technological Innovation Center, Zhejiang University, Hangzhou 311200, China

Correspondence to: Zhibin Wang (wangzhibin@zju.edu.cn) and Yuzhong Zhang (zhangyuzhong@westlake.edu.cn)

Abstract. Wastewater treatment plants (WWTPs) are substantial contributors to greenhouse gas (GHG) emissions because of the high production of methane (CH_4) and nitrous oxide (N_2O). A typical WWTP complex contains multiple functional areas that are potential sources for GHG emissions. Accurately quantifying GHG emissions from

these sources is challenging due to the inaccuracy of activity data, the ambiguity of emission sources, and the absence of monitoring standards. Locating and quantifying WWTPs emission sources using measurement-based GHG emission quantification method is crucial for evaluating and improving traditional emission inventories. In this study, CH_4 mobile measurements were conducted within a WWTP complex in the summer and winter of 2023. We utilized a multi-source Gaussian plume model combined with the genetic algorithm inversion framework, designed to locate major sources within the plant and quantify the corresponding CH_4 emission fluxes. We identified 13 main sources in the plant and estimated plant-scale CH_4 emission fluxes of 68.78 ± 17.40 kg h^{-1} (603.33 ± 152.66 t a^{-1}) for the summer and 47.76 ± 21.39 kg h^{-1} (418.95 ± 187.59 t a^{-1}) for the winter. The predominant sources of CH_4 emissions were the screen and primary clarifier, contributing 55 % and 67 % to the total emissions in summer and winter, respectively. The comparison revealed that summer CH_4 emissions were 2.8 times higher than inventory estimates, while winter emissions were twice the inventory values. This study demonstrated that mobile measurements, combined with the multi-source Gaussian plume inversion framework, are a powerful tool to locate and quantify GHG sources in a complex site, with the potential for further refinement to accommodate different types of factories and gas species.

1 Introduction

Methane (CH_4) is the second-largest contributor to climate change, with the global warming potential 27.9 times that of carbon dioxide (CO_2). Reducing CH_4 emissions is essential for mitigating climate change and progressively achieving the global target of limiting warming to 1.5 °C (IPCC, 2023). WMO Global Atmospheric Watch network indicated that the global annual average concentration of CH_4 in 2022 was 1923 ± 2 ppb, representing a 264 % increase from pre-industrial levels (WMO, 2023). The International Energy Agency (IEA) 2024 Global Methane Tracker report suggests that

global CH_4 emissions reached 580 Mt in 2023, with anthropogenic CH_4 emissions accounting for 60 %. The complexity of CH_4 emission processes, lack of monitoring systems, and limitations of emission estimation models present challenges in accurately estimating anthropogenic CH_4 emissions.

The quantification of CH_4 emission fluxes is typically achieved through a bottom-up inventory method. However, due to the difficulties in obtaining activity data used for actual emission factors, and specific information on different emission sources, there is considerable uncertainty in the assessing of the emission inventory method (Lin et al., 2021). In contrast, a top-down method that estimates CH_4 emissions by monitoring atmospheric concentration has been increasingly applied in recent years (Sun et al., 2019; Cusworth et al., 2024; Han et al., 2024; Maazallahi et al., 2023; Riddick et al., 2017). The monitoring technology mainly includes satellite (Zhang et al., 2021; Liang et al., 2023; Jacob et al., 2022) and airborne (Allen et al., 2019; Abeywickrama et al., 2023; Cui et al., 2017) remote sensing, as well as ground-based monitoring such as vehicle-based mobile monitoring (Albertson et al., 2016; Al-Shalan et al., 2022; Caulton et al., 2018), station monitoring (Dietrich et al., 2021; Hase et al., 2015; Heerah et al.,2021) and tower monitoring (Richardson et al., 2017; Balashov et al., 2020). Emission flux inversion methods also include isotope tracer method (Jackson et al., 2014; Zimnoch et al., 2018), cross-sectional flux method (Luther et al., 2019; Makarova et al., 2021), and atmospheric diffusion model inversion method (Kumar et al., 2021; Yacovitch et al., 2015). Atmospheric transport models with varied degrees of complexity, including Gaussian diffusion models (Stadler et al., 2021), Lagrangian models (Mckain et al., 2015), and Eulerian models (Bergamaschi et al., 2018), are used in the inversion to relate GHG concentrations with emissions. Optimization methods, such as Bayesian optimization (Karion et al., 2019) and linear regression models (Kumar et al., 2021), are applied to achieve accurate inversion results. Furthermore, some studies incorporate carbon isotope observations to better attribute the contribution of different CH_4 emission sources (Maazallahi et al., 2020). Numerous studies use

satellite remote sensing, unmanned aerial vehicle (UAV) monitoring, and vehicle-based mobile monitoring techniques to measure CH_4 emissions (Sun et al.,2023). However, satellite spatiotemporal resolution is limited and UAVs have short endurance, making vehicle-based mobile monitoring a better choice for measuring CH_4 emissions. Vehicle-based mobile monitoring can perform continuous real-time monitoring and precise identification of emission sources, and hence have been applied to urban (von Fischer et al., 2017; Defratyka et al., 2021) and plant-scale (Zhao et al., 2021; Jin et al.,2010) monitoring of GHG concentrations and emission fluxes. Vogel et al. (2024) used high-precision fast-response GHG analyzers to investigate CH_4 leaks in 12 cities across 8 countries. Chen et al. (2020) utilized the multiple-Gaussian-plume model for mobile measurements of CH_4 emissions during the Munich Oktoberfest. Shi et al. (2023) conducted mobile measurements with vehicle-based monitoring system at chemical, coal washing, and waste incineration plants in two cities and one industrial park in China.

As a significant source of GHG emissions, wastewater treatment plants (WWTPs) generate substantial amounts of CH_4, N_2O, and CO_2 during the collection, treatment, and discharge of sewage and sludge, contributing 3 % of the global total GHG emissions (Bai et al., 2022). The estimation of CH_4 emission fluxes from WWTPs has increasingly attracted widespread attention. Li et al. (2024) developed a plant-level and technology-based CH_4 emission inventory for municipal WWTPs in China, estimating the CH_4 emissions for 2020 to be 150.6 Gg. Delre et al. (2017) measured the CH_4 concentrations downwind of five WWTPs in Scandinavia using tracer gas dispersion, which obtained a range of CH_4 emission fluxes from 1.1 ± 0.1 to 18.1 ± 6.3 kg h^{-1}. Moore et al. (2023) employed CH_4 mobile measurements from 63 WWTPs in the United States, pointing to a significant underestimation in the CH_4 emission inventories. However, most studies lack comparisons between measured and simulated concentrations, resulting in significant uncertainty in the results. We present a mobile measurement investigation of a WWTP in Hangzhou 2023. To analyze the mobile data,

we construct a multi-source Gaussian plume model combined with the genetic algorithm inversion framework, which assists us to locate and quantify CH_4 emission sources, based on the concentration distribution measured within the WWTP. Additionally, we compare CH_4 emission fluxes from the measurements with the bottom-up estimates of emission inventories. A sensitivity analysis is performed to elucidate the discrepancies arising from variations in emission source locations. Our results provide insight into formulating and evaluating emission reduction measures for WWTPs.

2 Instruments and methods

2.1 Site selection

The monitoring site was chosen at a WWTP in Hangzhou, a megacity in East China. This WWTP is a large-scale plant located in Hangzhou, processing up to 1.5 million tons of domestic wastewater daily. The chosen WWTP processes encompass mechanical treatment, biological treatment, sedimentation, advanced treatment, disinfection, and sludge treatment. As illustrated in Fig. 1, we divide the WWTP into 14 functional areas according to treatment processes. Areas associated with primary treatment were labeled as coarse screens and primary sedimentation tanks, while those linked to secondary treatment were indicated as aeration tanks and secondary sedimentation tanks. We performed one monitoring experiment per day, with each experiment entailing 1-2 rounds of mobile measurements along external roads and internal functional areas roads. Additionally, we conducted repeated mobile measurements and fixed measurements on roads with high concentrations to calculate average concentration data. Over 10 days of experiments from June to December 2023, we obtain 8 days of complete monitoring data, including 3 days in summer and 5 days in winter. On the other two experimental days, internal facility maintenance restricted

access to certain roads, resulting in incomplete monitoring data.

Figure 1. Distribution of functional areas of the WWTP. The yellow mark represents the simulated location of the line source. Solid lines show the roads measured by the mobile vehicle. Map data are from ESRI.

2.2 Instrumentation

The monitoring instruments consisted of a vehicle-mounted Cavity Ring-Down Spectrometer (CRDS) monitoring system (Zhao et al., 2024) and a portable meteorological station. The vehicle-mounted CRDS system was anchored by the CRDS analyzer (Picarro G2201-i, Picarro 2010), accompanied by GPS and meteorological instruments. The volume fraction of CH_4 is measured with an accuracy of 5 ppb ± 0.05 %. CRDS measurements have the advantages of strong interference resistance, high sensitivity and accuracy, making them widely employed in research focused on monitoring GHG emissions (Rella et al., 2015; Lopez et al., 2017).

In this study, the CRDS analyzer was placed inside the monitoring vehicle to measure CH_4 concentrations in the WWTP. The sampling probe was placed near the roof along the window of the car to avoid interference from vehicle exhaust due to the low position.

The mobile meteorological instrument was placed on the roof of the vehicle to gather meteorological data. In addition, the GPS unit was integrated to record the location of sampling points during the measurement period. Two portable meteorological stations (Hangzhou Pengpu Technology SWS-500) were positioned adjacent to the main entrance and atop the filter tank at the WWTP. Capable of measuring meteorological parameters (wind speed, direction, temperature, humidity, and atmospheric pressure).

2.3 Inventory accounting method

We used the methods suggested by the IPCC Guidelines for National Greenhouse Gas Inventories (2006) to calculate the amounts of CH_4 emissions from wastewater. The formula for calculating the amounts of CH_4 emissions from wastewater is described as:

$$E_{CH_4} = (TOW - S \cdot a) \cdot EF_{CH_4} - R_{CH_4} \quad (1)$$

Where E_{CH_4} denotes the direct CH_4 emissions from the wastewater treatment plant, $tCH_4\ a^{-1}$. *TOW* is defined as the total organic pollutant load in the influent wastewater, $tCOD\ a^{-1}$. *S* refers to the annual production total of dry sludge, $t\ a^{-1}$. The parameter *a* signifies the organic matter content in the dry sludge, $tCOD\ t^{-1}$. EF_{CH_4} is the CH_4 emission factor, $tCH_4\ tCOD^{-1}$. R_{CH_4} quantifies the annual recovery of CH_4 from anaerobic treatment processes, $t\ a^{-1}$.

Operational data of the WWTP examined in this study is derived from the Urban Drainage Statistical Yearbook, an annual publication of urban water supply and drainage systems in China. This data set includes details such as the water treatment volume, sludge production, and the concentrations of six pollutants (COD_{Cr}, BOD, SS, NH_3-N, TN, and TP) in both influent and effluent. The Total Organic Waste (TOW) is calculated by the amount of treated water and COD influent concentration of the WWTP provided in the yearbook, while the annual sludge production (S) is extracted directly from the yearbook. The organic matter content in dry sludge is estimated at an

empirical 40 %, assuming a sludge moisture content of 75 %, leading to a value of 0.1 (Guo et al., 2019). EF_{CH_4} is selected based on the recommended value for Zhejiang province, 0.0046 (Cai et al., 2015). Given the infrequency of anaerobic treatment in wastewater, R_{CH_4} is set to 0.

2.4 Inversion method

We developed an inversion framework for emission fluxes designed for plant-level applications. The framework used mobile measurements data, locations of emission sources, and initial emission estimates, alongside wind speed and direction data, as inputs to the multi-source Gaussian diffusion models. The preliminary localization of the emission sources was chiefly contingent upon the concentration distribution along the roads within the internal functional areas. Meanwhile, the initial emission estimates for each source were determined by integrating the concentration data from these areas with an improved empirical equation (Weller et al., 2019). Based on the comparison of measurement and model simulation results (Fig. S1), it is determined that the plant exhibits multiple point sources and line source diffusion patterns. Fig. S1 illustrates that the CH_4 concentration curve presents distinct peak distributions in point source diffusion patterns, while the CH_4 concentration distribution in line source diffusion patterns consistently maintains higher levels. We then used a genetic algorithm to iteratively optimize source emission fluxes and their locations. The inversion framework simulation dictated the placement of 12 main point sources throughout the WWTP, specifically within Aeration Tank ①②③④⑤, Primary Clarifier ③④⑤, Screen ①, Secondary Clarifier ①②, and the Sludge Treatment ② (Fig. 1). Within this study, a uniform line source was established, with the assumed location along the road between the Screen ① and the Primary Clarifier ① (Fig. 1 yellow mark). This assumption was grounded in the CH_4 concentration distribution observed within this

road segment and was substantiated through model validation. The remaining emission flux inversion processes followed the same procedure as the point source simulation. Adjustments to the source locations within the model narrow the gap between simulated and measured concentrations, thus enhancing the accuracy of inversion. This section delineates each model incorporated into the inversion framework.

2.4.1 Empirical equation for estimating initial emissions

We used the improved empirical equation to estimate the initial emissions of emission sources (von Fisher et al., 2017; Weller et al.,2019). This method was primarily utilized for urban CH_4 leakage source emissions estimation (Defratyka et al., 2021; Maazallahi et al., 2020). The empirical equation is as follows:

$$ln\left(M_{CH_4}\right) = -0.988+0.817\times ln\ (CH_4\ emission\ rate) \quad (2)$$

The M_{CH_4} is the maximum enhancement value of CH_4 concentration, ppm. The $CH_4\ emission\ rate$ represents the CH_4 emission flux, L min^{-1}.

2.4.2 Multiple-point-source Gaussian plume model

We developed a multiple-point-source Gaussian plume model to relate CH_4 concentration enhancement to CH_4 emissions. This method approximates atmospheric dispersion of CH_4 from an individual source as a Gaussian plume under uniform and stable wind conditions (Nassar et al., 2017), which is usually good for describing average atmospheric transport tens to hundreds of meters downwind the source, making the Gaussian plume model a useful tool to study emissions from industrial and traffic sources.

The mass concentration enhancement (C, mg m^{-3}) is computed as superposition of Gaussian plumes from multiple point sources.

$$C(x,y,z) = \sum_{i=1}^{n} \frac{Q_i}{2\pi\bar{u}\sigma_{i,y}\sigma_{i,z}} exp\left(-\frac{(y-y_i)^2}{2{\sigma_{i,y}}^2}\right)\left\{exp\left[\frac{-(z-z_i)^2}{2{\sigma_{i,Z}}^2}\right] + exp\left[\frac{-(z+z_i)^2}{2{\sigma_{i,Z}}^2}\right]\right\} \quad (3)$$

The variables x, y, and z denote the downwind, crosswind distances, and the height

above the ground from the source, m. Q_i signifies the emission rate from the i_{th} point source, mg s^{-1}, for i = 1, 2, 3……N, where N represents the total count of point sources. The average wind speed is indicated by $\bar{u}$, m s^{-1}. The x_i, y_i and z_i are represented as the spatial position of the i_{th} point source, m. $\sigma_{i,y}$ and $\sigma_{i,Z}$ are the horizontal and vertical dispersion parameters of the i_{th} point source, respectively, which are given by the formula below:

$$\sigma_{i,y} = \gamma_1 \cdot (x - x_i)^{\alpha_1},\ when\ x > x_i \quad (4)$$

$$\sigma_{i,z} = \gamma_2 \cdot (x - x_i)^{\alpha_2},\ when\ x > x_i \quad (5)$$

The power functions, known as the Pasquill's curves, associates with the downwind distance x and the prevailing atmospheric stability (Briggs et al., 1973). Atmospheric stability is determined based on the Pasquill stability classes recommended in the Technical Principles and Methods for Formulating Local Air Pollution Emission Standards (GB3840-83). During the observation, the CH_4 concentrations were obtained through the vehicle-mounted CRDS monitoring system. The portable meteorological stations collected data on wind speed and direction, while GPS tracked the mobile paths to pinpoint emission source locations.

2.4.3 General Finite Line Source Model

Our analysis of measurement at WWTPs indicates that multiple-point-source Gaussian plume model is insufficient to capture the observed CH_4 concentrations. The entire road between the Screen ① and the Primary Clarifier ① shows high distribution of CH_4 concentrations. The contribution of a line source to CH_4 concentration is given by the General Finite Line Source Model (GFLSM) (Luhar et al., 1989; Venkatram et al., 2006), which represents the line source as an ensemble of point sources:

$$C = \frac{Q}{2\pi\bar{u}\sigma_y\sigma_z}\left\{exp\left[\frac{-(z-H)^2}{2{\sigma_Z}^2}\right] + exp\left[\frac{-(z+H)^2}{2{\sigma_Z}^2}\right]\right\}$$

$$\cdot \left[erf\left(\frac{\sin\theta\left(\frac{L}{2}-y\right)-x\cos\theta}{\sqrt{2}\sigma_y} \right) + erf\left(\frac{\sin\theta\left(\frac{L}{2}+y\right)+x\cos\theta}{\sqrt{2}\sigma_y} \right) \right] \quad (6)$$

x, y, and z correspond to the downwind, crosswind distances, and the altitude above ground level from the source, m. Q_i is the emission fluxes of the unit source, mg s^{-1}. $\bar{u}$ is the average wind speed, m s^{-1}. H_i is the effective emission height of the line source, with the length of the line source represented by L, m. The angle between the line source and the wind direction is given by θ. The horizontal and vertical dispersion parameters are characterized by σ_y and σ_z, respectively.

2.4.4 Genetic algorithm

Genetic algorithms, which mimic the evolutionary process of biological systems, serve as optimization search algorithms. The algorithms encode practical problems into binary genetic coding. Through the simulation of natural selection, crossover, and mutation processes, these algorithms are in a constant state of evolution and iteration, all in the pursuit of the optimal solution (Katoch et al., 2021). We deployed genetic algorithms to enhance the source emission flux outcomes modeled by the Gaussian plume model.

The process of inverting multi-source CH_4 emission fluxes utilizing genetic algorithms involves a series of steps. Initially, the emission flux of each source is treated as a gene, with binary-encoded gene sequences randomly assigned to a set number of individuals within the predefined range of a priori emission fluxes. Subsequently, the formulation of a fitness function is based on the defined optimization goals and constraints. This function serves as a critical tool for assessing the relative merits of each individual within the population. In this study, the objective of the optimization is centered on minimizing the aggregate absolute discrepancy between the values predicted by the model and those obtained from measurements. Ultimately, the population is subjected to the processes of selection, crossover, and mutation.

Individuals with elevated fitness values, as determined by the fitness function, are chosen for the generation of new individuals. Through an iterative process, the optimal solution is refined, representing the emission fluxes for each source. Genetic algorithms are distinguished by the parallel computation capabilities, the propensity for identifying global optima, and the commendable stability and reliability (Harada et al., 2020).

2.4.5 Uncertainty analysis

To quantify the uncertainty in the inversion results, we have considered the uncertainties associated with the input parameters of the inversion model, including wind speed, wind direction, and instrument measurements. The uncertainty in the CH_4 emission fluxes (ε_t) is derived using the error propagation formula as follows:

$$\varepsilon_t = \sqrt{{\varepsilon_s}^2 + {\varepsilon_d}^2 + {\varepsilon_m}^2} \quad (7)$$

ε_s and ε_d denote the uncertainties in wind speed and direction, which are determined by the standard deviation of the wind speed and direction measurements from two fixed meteorological stations during the observation period. ε_m represents the uncertainty in instrumental measurements. This uncertainty is derived from data provided by the manufacturer Picarro, which indicates a concentration measurement uncertainty of approximately 1 ppb for a 10-second integration time (Picarro 2010).

3 Results and discussion

3.1 Concentration mapping

The closed-path mobile measurements were conducted by vehicle-mounted CRDS monitoring system along the external roads encircling the WWTP, with further monitoring conducted along the internal roads. This strategy depicts the distribution of CH_4 concentrations within an WWTP, allowing for identification of specific CH_4 emission sources. Based on 8 days of CH_4 monitoring experimental data, the CH_4

concentration range on the overall roads was determined to be 1.98-17.13 ppm. The CH_4 concentration distribution indicated higher levels downwind, with the highest concentrations consistently recorded at the Screen ① throughout mobile experiments.

Due to the consistency of concentration measurement methods, we chose 29th June and 13th December as a typical example. Figure 2 illustrates measured CH_4 concentration enhancement distributions on 29th June (summer) and 13th December (winter) 2023 (other days are shown in Figures S3-S8). The CH_4 concentration enhancements depicted were calculated by subtracting the background concentrations from the measured values, with the background determined as the mean of the bottom 10 % of the concentration data. Specifically, the background concentrations register at 1.98 ppm on 29th June and at a slightly elevated 2.11 ppm on 13th December. The analysis indicates that the shallower boundary layer in winter causes CH_4 to accumulate near the surface, resulting in a higher background concentration. Moreover, increased concentrations are detected in the regions surrounding the Screen ①, Primary Clarifier ④, and Aeration Tank ③ during these two days. The complete concentration maps , which include the internal roads, reveal that the experiment on 29th June exhibits heightened concentrations at the Screen ①, Secondary Clarifier ②, and Primary Clarifier ②④. The Screen ① exhibits the highest CH_4 concentration, with an enhancement of 14.83 ppm. On 13th December, the concentration enhancements are noted in proximity to the Secondary Clarifier ① and Primary Clarifier ②, with the Primary Clarifier ② showing the highest CH_4 concentration at 4.79 ppm.

CH_4 concentrations in summer surpass those observed in winter, consistent with a previous study on WWTPs (Masuda et al., 2015). The screen, primary clarifier and aeration tank are identified as sources with notably higher concentrations. Analysis of concentration distributions reveals that Screen ① shows a peak concentration reaching

14.83 ppm, which is 7.5 times the background concentration. The four primary clarifiers record high concentrations between 4.79 and 10.88 ppm. The high value measured by aeration tanks is mainly detected in Aeration Tank ③ at 4.60ppm. The screen in this study includes coarse and fine screens and a grit chamber, constituting preliminary wastewater treatment to capture larger suspended solids and particulates. The anaerobic environment of the sewer network promotes the production of CH_4 from organic compounds in municipal wastewater. As this wastewater enters the WWTP, the influent contains dissolved CH_4 that originated in the sewer network. During primary treatment, wastewater is elevated through riser mains, facilitating the release of CH_4 into the atmosphere (Guisasola et al., 2008; Bao et al., 2016). Flow velocity, hydraulic design and detention times in these facilities may affect CH_4 production and release (Alshboul et al., 2016; Yin et al., 2024). The primary clarifier physically removes suspended solids from wastewater through sedimentation, while organic matter undergoes anaerobic microbial degradation to the substantial production of CH_4 (Masuda et al., 2017). In the aeration tank, operated under anaerobic and anoxic conditions, complex organic compounds are converted to CH_4 by facultative and anaerobic bacteria through biological processes (Yoshida et al.,2014). In contrast, Kupper et al. (2018) identified sludge storage tanks as the primary source of CH_4 emissions in Swiss WWTPs, accounting for 70 % or more of the total emissions. Stadler et al. (2022) monitored CH_4 concentrations inside and around wastewater treatment facilities ranging from 2.04-32.78 ppm, with elevated CH_4 levels predominantly measured near sludge treatment tank, the digesters and secondary clarifiers. CH_4 emissions from various WTTPs are affected by a range of factors, including specific processes, pipeline design, and equipment aging, the mobile monitoring can better reflect the actual emission distribution.

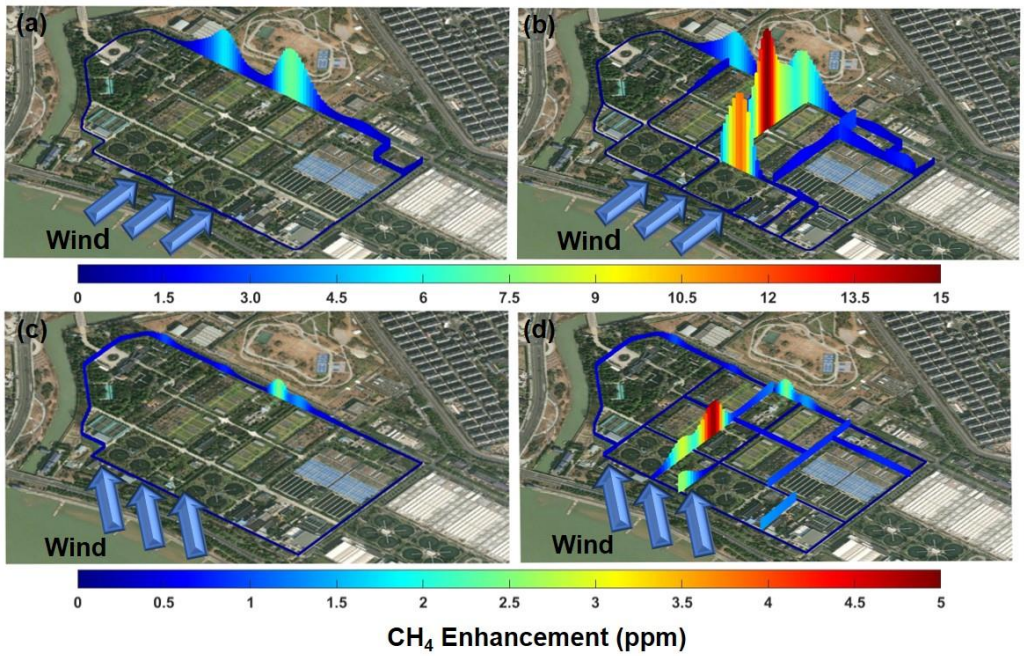

Figure 2. CH_4 concentration maps in the WWTP. The concentration maps for the external roads for 29th June (a) and 13th December (c). The corresponding complete concentration maps that include the internal roads for 29th June (b) and 13th December (d). Map data are from ESRI.

3.2 Emission quantification

The mobile measured CH_4 concentrations were employed in combination with the inversion framework to achieve the quantification of CH_4 emissions and localization of the emission sources within the WWTP. Figures 3 and 4 show the locations of identified point sources and the comparison between measured and simulated concentration distribution. The experiment conducted on 29th June finds the Screen ① to be the most significant contributor to CH_4 point source emissions at 18.26 kg h^{-1}, and the Secondary Clarifier ② as the least significant at 1.23 kg h^{-1}. The correlation coefficient R^2 for the measured and simulated concentrations is 0.63, with an RMSE of 0.70 mg m^{-3}. On 13th December, the Aeration Tank ⑤ is the largest point source of CH_4 emissions at 3.93

kg h^{-1}, and the Primary Clarifier ⑤ is the smallest at 0.55 kg h^{-1}, with a correlation coefficient R^2 of 0.70 and an RMSE of 0.28 mg m^{-3}. The enhanced correlation between winter measurement and simulation data, as well as the improved fit of the measurement and simulation value curves, is attributed to the shorter monitoring cycle and more stable meteorological conditions.

In addition, when employing the multi-source Gaussian diffusion model combined with a genetic algorithm framework for iterative optimization to pinpoint point sources, we were able to locate external sources. As shown in Fig. S2 (a) and (c), external sources are primarily located along the main roadway to the south of the WWTP. Moreover, the estimated emissions vary across different days, which indicates that external source emissions are influenced by traffic vehicles. Fig. S2 (b) and (d) compare measured and simulated CH_4 concentrations before and after accounting for external sources, demonstrating that simulations are significantly closer to the measurements when external sources are included.

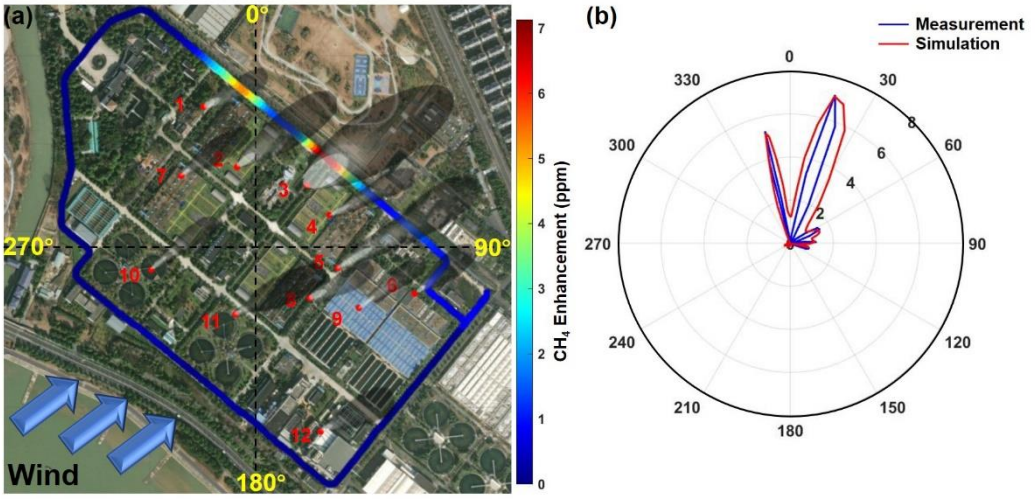

Figure 3. The emission distribution for the source locations (a) and the comparison between measured and simulated CH_4 concentrations (b) at the WWTP on 29th June. Map data are from ESRI.

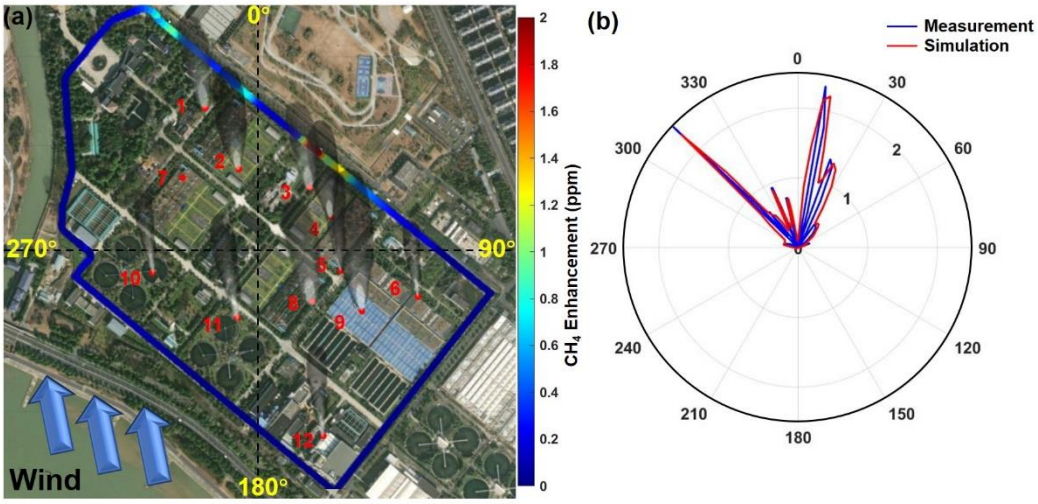

Figure 4. The emission distribution for the source locations (a) and the comparison between measured and simulated CH_4 concentrations (b) at the WWTP on 13th December. Map data are from ESRI.

Table 1 displays the CH_4 emission fluxes (Q), Wind speed and direction data (W_s, W_d), the horizontal diffusion coefficient (γ_1, α_1) and the vertical diffusion coefficient (γ_2, α_2) from the 8-day monitoring experiment. Wind speed and direction data are the average wind speed and direction during the monitoring time, and the CH_4 emission fluxes are obtained by the inversion of the average concentration, wind speed and direction data as input of the inversion framework. The emission flux values of CH_4 emission sources (12 point sources and 1 line source) for all experimental days are detailed in Tables S1 and S2. It is observed that the summer average CH_4 emission flux (68.78 ± 17.40 kg h^{-1}) surpasses the winter average CH_4 emission flux (47.76 ± 21.39 kg h^{-1}). This seasonal disparity in emissions is primarily attributed to the aeration tank, followed by the screen and primary clarifier. The activated sludge in the aeration tank contains a higher population of methanogens, whose CH_4 production capability intensifies with rising temperatures (Vítěz et al., 2020). Notably, the seasonal variance in the aeration tank is predominantly driven by the performance of the Aeration Tank ④. However, the substantial variation in the emissions from the three summer

experiments of the Aeration Tank ④ suggests a degree of emission instability. Conversely, the uniformity in the low emissions from the five winter experiments might be associated with the meteorological conditions and the actual operational status of the plant on those days. At lower wind speeds, the CH_4 emissions show only slight differences when compared to emissions on days with higher wind speeds. This suggests that the inversion results are less influenced by wind speed and are primarily associated with seasonal variations.

The screen and primary clarifier are the predominant emission sources at the WWTP. Specifically, these sources emit 37.50 kg h^{-1} in the summer and 31.92 kg h^{-1} in the winter, accounting for 55 % and 67 % of the total emissions. Pipeline leaks near the screen and primary clarifier lead to the CH_4 release. Previous research has similarly examined major emission sources at WWTPs. Yin et al. (2024) conducted offline monitoring of WWTPs in Beijing and Guiyang, identifying the primary treatment zone as the primary source of CH_4, accounting for 60.1 % and 35.8 % of the respective total emissions. Masuda et al. (2017) analyzed CH_4 emissions from different processes at three WWTPs in Japan, concluding that primary clarifiers are one of the major sources of CH_4 emissions. He et al. (2023) compiled CH_4 emission proportions for different processes in WWTPs based on reported data, finding percentages of 7 %-12 % for grit chamber, 8.2 %-68.1 % for primary clarifier, and 18.3 %-86.4 % for aeration tank.

Table 1. CH_4 emission fluxes (Q), Wind speed and direction data (W_s, W_d), the horizontal diffusion coefficient (γ_1, α_1) and the vertical diffusion coefficient (γ_2, α_2) from the 8-day monitoring experiment.

Date	Q (kg h^{-1})	W_s (m s^{-1})	W_d (°)	γ_1	α_1	γ_2	α_2
0601	61.85 ± 20.41	2.3	248.5	0.28	0.91	0.13	0.94
0629	74.92 ± 35.21	1.9	238.3	0.28	0.91	0.13	0.94
0711	69.58 ± 32.70	0.9	225.8	0.28	0.91	0.13	0.94

1213	49.19 ± 21.15	1.6	175.7	0.28	0.91	0.13	0.94
1214	43.29 ± 27.28	1.2	209.9	0.28	0.91	0.13	0.94
1220	49.99 ± 25.00	3.8	342.3	0.18	0.92	0.11	0.92
1221	48.17 ± 17.34	2.7	342.6	0.43	1.10	0.08	1.12
1222	48.15 ± 21.67	3.0	342.5	0.43	1.10	0.08	1.12

An alternative top-down approach known as the tracer gas dispersion method (TDM), which has been applied to estimate CH_4 emissions from city streets (von Fischer et al., 2017; Weller et al., 2018), WWTPs (Yoshida et al., 2014; Delre et al., 2017; Delre et al., 2018), biogas plants (Reinelt et al., 2017; Scheutz et al., 2019; Fredenslund et al., 2023) and landfills (Rees-White et al., 2019; Kissas et al., 2022). TDM involves releasing tracer gases like nitrous oxide and acetylene near the source and measuring their concentrations along with CH_4 downwind using a mobile platform. The similar diffusion patterns of CH_4 and the tracer gases result in a stable concentration ratio after atmospheric mixing, enabling the calculation of CH_4 emission rates with a better accuracy (Mønster et al., 2014).

Moreover, the TDM was employed to validate and compare other model inversion methods. Moore et al. (2023) proposed that the Gaussian dispersion modeling demands less experimental equipment, site access, and manpower than the TMD, which allows for swifter data gathering. Yacovitch et al. (2015) utilized a five-day dataset of tracer gas release in the Barnett shale region to evaluate the Gaussian dispersion flux quantification method. The results indicated a 95% confidence interval, with a lower bound factor of 0.334 and an upper bound factor of 3.34. von Fischer et al. (2017) performed three controlled release experiments to validate the reliability of leak rate algorithm in Fort Collins, CO, which indicated a very significant correlation between known and estimated leak rates ($p < 0.0001$, $r^2 = 0.43$). Compared to the method employed in the study, the TDM offers advantages such as simpler formula calculations. Nonetheless, it also presents several drawbacks, including complex experimental

procedures, safety hazards associated with the release of tracer gases, which require access permits from industrial facilities.

3.3 Comparison with IPCC method

The CH_4 emissions were also calculated using the IPCC method, with data sourced from the Urban Drainage Statistical Yearbook of 2017. The emission flux of 213.95 ± 128.37 t a^{-1} was determined, with the uncertainty (60%) derived from the data summarized in the research (Lin et al., 2021). Figure 5 shows the contrast between the emission inversion results from the monitoring experiment and the emission inventory. The uncertainty of the inversion results was determined by accounting for the uncertainties in wind speed, wind direction, and instrument measurements, following the method presented in Section 2.4.5. The uncertainties in emission fluxes inversion ranged from 33% to 63% on individual days. Notably, the uncertainty associated with wind speed contributes approximately 44% to 94% of the uncertainty range. The summer average inversion emission flux (603.33 ± 152.66 t a^{-1}) was calculated to be 2.8 times that of the inventory, and the winter average (418.95 ± 187.59 t a^{-1}) was twice as much. It is posited that the discrepancy may stem from significant uncertainties in the emission factors associated with the WWTPs or the lack of updated activity level data, as the statistical yearbook provided data only up to 2017, the emission inventory might have underestimated the actual emissions.

Furthermore, other studies have also investigated the comparison between CH_4 emissions obtained from different measurement methods at WWTPs and IPCC inventory estimates. The majority of these studies indicate that the measured values exceed the inventory values. Wang et al. (2021) conducted a measurement-based assessment of CH_4 emissions (46.58 t a^{-1}) in Wuhu City, revealing a 46.71 % higher than those calculated using the IPCC method. Moore et al. (2023) employed mobile monitoring to evaluate CH_4 emissions at 63 WWTPs across the

United States. Specifically, CH_4 emissions from centrally treated domestic wastewater in the U.S. amount to 4.64×10^5 t a^{-1}, which is 1.9 times greater than the EPA inventory. Song et al. (2023) investigated CH_4 emissions from municipal wastewater treatment in the U.S at $(4.36 \pm 2.8) \times10^5$ t a^{-1}. This value was approximately twice the estimates provided by the IPCC. Our estimated results are generally consistent with the previous studies. The lower estimated results provided by the IPCC method can be attributed to the neglect of certain potential emission sources from the emission inventories, including emissions from equipment in sludge treatment facilities and leaks from pressure relief valves.

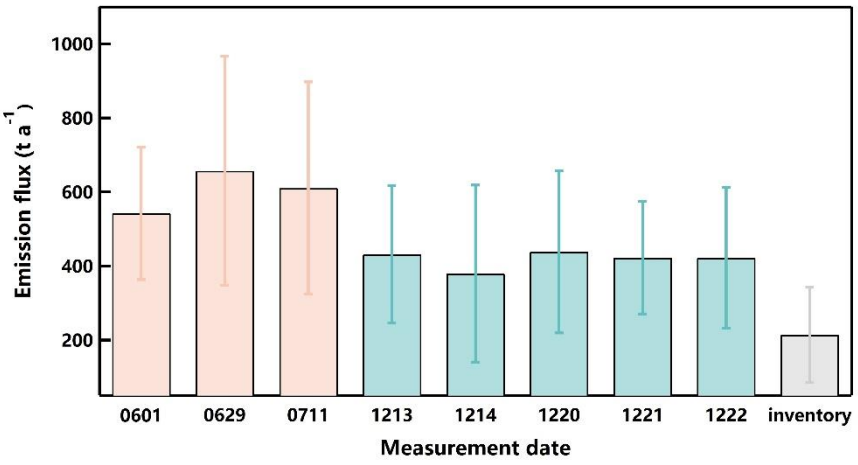

Figure 5. Comparison of CH_4 emission fluxes from the monitoring experiment and emission inventory in the WWTP.

3.4 Sensitivity analysis

In this section, we evaluated the stability of the inversion framework through sensitivity analysis and explored the impact of different point source locations on the inversion of emission concentrations. The precise identification of emission sources can enhance the accuracy of emission flux inversion, making a sensitivity analysis of the source location essential. We applied the method of controlling variables to perform a sensitivity analysis on the location of a single point source. The central position of the

plant was taken as the reference origin, the positions of 12 emission sources were determined to analyze the variation in error between measured and simulated concentrations within a 200 m × 200 m range around each emission source. We sequentially modified the source position parameters in the model input to analyze the congruence between the simulated concentrations and the observed measurements, quantifying the fit with RMSE. The change in concentration error serves as an indicator of the accuracy of the emission source localization.

Figures 6 and 7 describe the error variation between monitored and simulated concentrations when the point source location is subject to change within a 200 m × 200 m range from the monitoring experiment on 29th June and 13th December. The error variation of the remaining days can be seen in Figures S9-S14. The point source locations simulated based on the inversion framework are mostly in areas with minor relative concentration errors, which can be considered to have a high reliability in simulating point source locations. The emission source location errors for the two experiments are within the ranges of 0.7-1.3 mg m^{-3} and 0.2-0.3 mg m^{-3}. The winter emission source locations exhibit greater stability and accuracy in the inversion results than the summer ones.

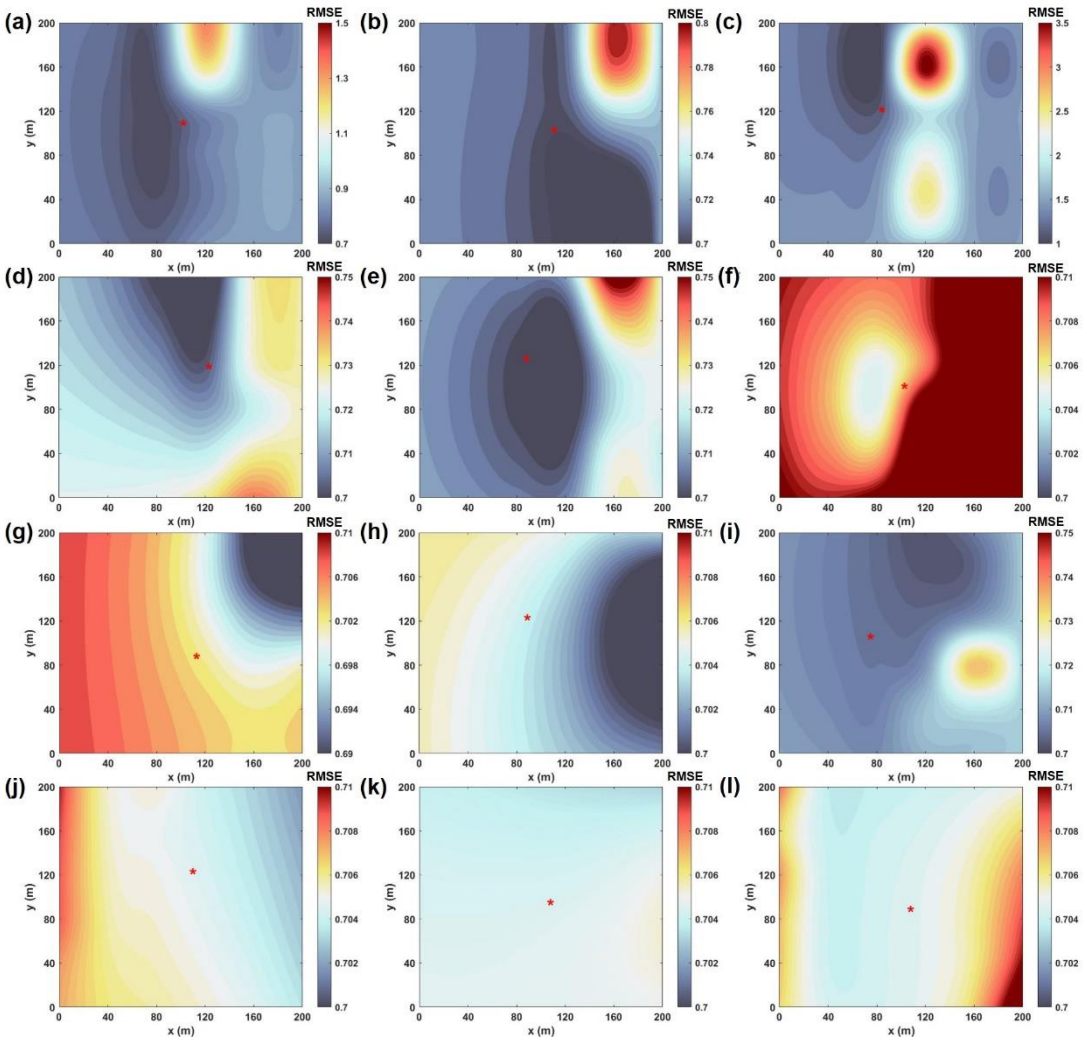

Figure 6. RMSE of monitoring simulated concentration changes with the location of WWTP source on 29th June. The x and y axes denote the horizontal and vertical distances of the simulated point source from the central point of the WWTP. The variation in color signifies the alteration in the root mean square error between the actual monitored and simulated concentrations, with the red star symbolizing the simulated point source location.

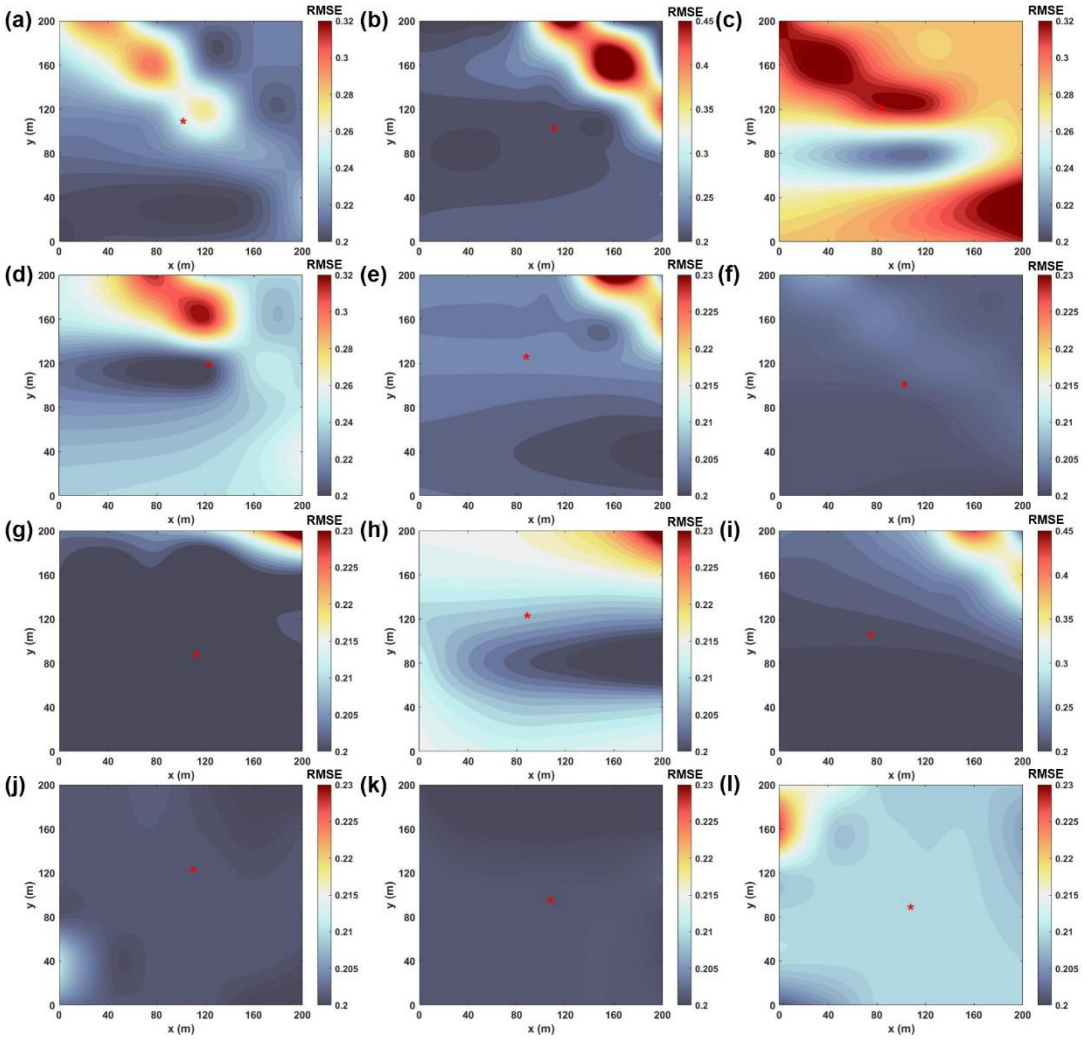

Figure 7. RMSE of monitoring simulated concentration changes with the location of WWTP source on 13th December.

4 Conclusions and outlook

The study carried out mobile measurements at a WWTP across the summer and winter seasons from Hangzhou 2023. By employing a multi-source Gaussian plume model combined with the genetic algorithm inversion framework, the inversion of CH_4 emission fluxes and their source locations was achieved. The results showed that 12 distinct CH_4 emission sources were pinpointed. The average CH_4 emission flux during the summer was 68.78 ± 17.40 kg h^{-1} (603.33 ± 152.66 t a^{-1}), and 47.76 ± 21.39 kg h^{-1} (418.95 ± 187.59 t a^{-1}) for the winter. The screen and primary clarifier were the main

sources, accounting for 55 % of summer and 67 % of winter emissions. The summer CH_4 inversion emissions were found to be 2.8 times higher, and the winter inversion emissions were twice as much as the inventory-based estimation.

The inversion framework is capable of validating emission coefficients in the inventory, identifying emission sources within the plant, and monitoring abnormal emissions. It can be applied to various monitoring systems, such as UAV systems and networks of fixed monitoring stations. We believe that it is an excellent point that collaborative monitoring offers significant improvements in the accuracy of emission fluxes and source inversion. Future efforts should aim to refine the inversion framework for broader applicability to various pollutant gases, enhancing the inversion efficiency, and extending the validation of the framework through monitoring experiments in a diverse range of industrial facilities.

Data availability. The raw data in this paper can be obtained from the corresponding author upon request.

Author contributions. ZW and YZ administrated the project and determined the main goal of this study. ZX, JY and XP designed the methods and planned the campaign. JY, ZX, YY, SZ and BQ performed the measurements. JY wrote the paper with contributions from all co-authors.

Competing interests. At least one of the (co-)authors is a member of the editorial board of Atmospheric Chemistry and Physics.

Financial support. The study has been supported by the National Key Research and Development Program of China (grant nos. 2022YFC3703500 and 2022YFE0209100), the National Natural Science Foundation of China (grant no. 42307129), the Key Research and Development Program of Zhejiang Province (grant nos. 2021C03165 and 2022C03084), the Zhejiang Provincial Natural Science Foundation (grant no. LZJMZ24D050005), and the Ecological Environment Research and Achievement

572 Promotion Project of Zhejiang Province (grant nos. 2024XM0053 and 2024XM0052).
573

574 **References**

575 Abeywickrama, H. G. K., Bajón-Fernández, Y., Srinamasivayam, B., Turner, D., and
576 Rivas Casado, M.: Development of a UAV based framework for CH_4 monitoring in
577 sludge treatment centres, Remote Sens., 15, 3704, https://doi.org/10.3390/
578 rs15153704, 2023.
579 Albertson, J. D., Harvey, T., Foderaro, G., Zhu, P., Zhou, X., Ferrari, S., Amin, M. S.,
580 Modrak, M., Brantley, H., and Thoma, E. D.: A Mobile Sensing Approach for
581 regional surveillance of fugitive methane emissions in oil and gas production,
582 Environ. Sci. Technol., 50, 2487-2497, https://doi.org/10.1021/acs.est.5b05059,
583 2016.Allen, G., Hollingsworth, P., Kabbabe, K., Pitt, J. R., Mead, M. I., Illingworth,
584 S., Roberts, G., Bourn, M., Shallcross, D. E., and Percival, C. J.: The development
585 and trial of an unmanned aerial system for the measurement of methane flux from
586 landfill and greenhouse gas emission hotspots, Waste Manage., 87, 883-892,
587 https://doi.org/10.1016/j.wasman.2017.12.024, 2019.
588 Al-Shalan, A., Lowry, D., Fisher, R. E., Nisbet, E. G., Zazzeri, G., Al-Sarawi, M.,
589 France, J. L.: Methane emissions in Kuwait: Plume identification, isotopic
590 characterisation and inventory verification, Atmos. Environ., 268, 118763,
591 https://doi.org/10.1016/j.atmosenv.2021.118763, 2022.
592 Alshboul, Z., Encinas-Fernández, J., Hofmann, H., and Lorke, A.: Export of dissolved
593 methane and carbon dioxide with effluents from municipal wastewater treatment
594 plants, Environ. Sci. Technol., 50, 5555-5563, https://doi.org/10.1021/acs.est.
595 5b04923, 2016.
596 Bai, R. L., Jin, L., Sun, S. R., Cheng, Y., and Wei, Y.: Quantification of greenhouse gas
597 emission from wastewater treatment plants, Greenhouse. Gas. Sci. Technol., 12, 587-
598 601, https://doi.org/10.1002/ghg.2171, 2022.

599 Balashov, N. V., Davis, K. J., Miles, N. L., Lauvaux, T., Richardson, S. J., Barkley, Z.
600 R., and Bonin, T. A.: Background heterogeneity and other uncertainties in estimating
601 urban methane flux: results from the Indianapolis Flux Experiment (INFLUX),
602 Atmos. Chem. Phys., 20, 4545-4559, https://doi.org/10.5194/acp-20-4545-2020,
603 2020.
604 Bao, Z., Sun, S., and Sun, D.: Assessment of greenhouse gas emission from A/O and
605 SBR wastewater treatment plants in Beijing, China. Int. Biodeterior. Biodegrad., 108,
606 108-114, https://doi.org/10.1016/j.ibiod.2015.11.028, 2016.
607 Bergamaschi, P., Karstens, U., Manning, A. J., Saunois, M., Tsuruta, A., Berchet, A.,
608 Vermeulen, A. T., Arnold, T., Janssens-Maenhout, G., Hammer, S., Levin, I., Schmidt,
609 M., Ramonet, M., Lopez, M., Lavric, J., Aalto, T., Chen, H., Feist, D. G., Gerbig, C.,
610 Haszpra, L., Hermansen, O., Manca, G., Moncrieff, J., Meinhardt, F., Necki, J.,
611 Galkowski, M., O'Doherty, S., Paramonova, N., Scheeren, H. A., Steinbacher, M.,
612 and Dlugokencky, E.: Inverse modelling of European CH_4 emissions during 2006–
613 2012 using different inverse models and reassessed atmospheric observations, Atmos.
614 Chem. Phys., 18, 901-920, https://doi.org/10.5194/acp-18-901-2018, 2018.
615 Cai, B., Gao, Q., Li, Z., Wu, J., Cao, D., and Liu, L.: Study on the methane emission
616 factors of wastewater treatment plants in China, China Population Resources and
617 Environment, 25, 118-124, https://doi.org/10.3969/j.issn.1002-2104.2015.04.015,
618 2015.
619 Caulton, D. R., Li, Q., Bou-Zeid, E., Fitts, J. P., Golston, L. M., Pan, D., Lu, J., Lane,
620 H. M., Buchholz, B., Guo, X., McSpiritt, J., Wendt, L., and Zondlo, M. A.:
621 Quantifying uncertainties from mobile-laboratory-derived emissions of well pads
622 using inverse Gaussian methods, Atmos. Chem. Phys., 18, 15145-15168,
623 https://doi.org/10.5194/acp-18-15145-2018, 2018.
624 Chen, J., Dietrich, F., Maazallahi, H., Forstmaier, A., Winkler, D., Hofmann, M. E. G.,
625 Denier van der Gon, H., and Röckmann, T.: Methane emissions from the Munich
626 Oktoberfest, Atmos. Chem. Phys., 20, 3683-3696, https://doi.org/10.5194/acp-20-

627 3683-2020, 2020.
628 Cui, Y. Y., Brioude, J., Angevine, W. M., Peischl, J., McKeen, S. A., Kim, S.-W.,
629 Neuman, J. A., Henze, D. K., Bousserez, N., Fischer, M. L., Jeong, S., Michelsen, H.
630 A., Bambha, R. P., Liu, Z., Santoni, G. W., Daube, B. C., Kort, E. A., Frost, G. J.,
631 Ryerson, T., Wofsy, S. C., and Trainer, M.: Top-down estimate of methane emissions
632 in California using a mesoscale inverse modeling technique: The San Joaquin Valley,
633 J. Geophys. Res., 122, 3686–3699, https://doi.org/10.1002/2016JD026398, 2017.
634 Cusworth, D. H., Duren, R. M., Ayasse, A. K., Jiorle, R., Howell, K., Aubrey, A., Green,
635 R. O., Eastwood, M. L., Chapman, J. W., Thorpe, A. K., Heckler, J., Asner, G. P.,
636 Smith, M. L., Thoma, E., Krause, M. J., Heins, D., and Thorneloe, S.: Quantifying
637 methane emissions from United States landfills, Science, 383, 1499-1504,
638 https://www.science.org/doi/10.1126/science.adi7735, 2024.
639 Defratyka, S. M., Paris, J. D., Yver-Kwok, C., Fernandez, J. M., Korben, P., and
640 Bousquet, P.: Mapping urban methane sources in Paris, France, Environ. Sci.
641 Technol., 55, 8583-8591, https://doi.org/10.1021/acs.est.1c00859, 2021.
642 Delre, A., Mønster, J., and Scheutz, C.: Greenhouse gas emission quantification from
643 wastewater treatment plants, using a tracer gas dispersion method, Sci. Total.
644 Environ., 605-606, 258-268, http://dx.doi.org/10.1016/j.scitotenv.2017.06.177, 2017.
645 Delre, A., Mønster, J., Samuelsson, J., Fredenslund, A. M., and Scheutz, C.: Emission
646 quantification using the tracer gas dispersion method: the influence of instrument,
647 tracer gas species and source simulation, Sci. Total. Environ., 634, 59-66,
648 https://doi.org/10.1016/j.scitotenv.2018.03.289, 2018.
649 Dietrich, F., Chen, J., Voggenreiter, B., Aigner, P., Nachtigall, N., and Reger, B.:
650 MUCCnet: Munich Urban Carbon Column network, Atmos. Meas. Tech., 14, 1111-
651 1126, https://doi.org/10.5194/amt-14-1111-2021, 2021.
652 Fredenslund, A. M., Gudmundsson, E., Falk, J. M., and Scheutz, C.: The Danish
653 national effort to minimise methane emissions from biogas plants, Waste Manag.,
654 157, 321-329, https://doi.org/10.1016/j.wasman.2022.12.035, 2023.

Guisasola, A., de Haas, D., Keller, J., and Yuan, Z.: Methane formation in sewer systems. Water Res., 42, 1421-1430, https://doi.org/10.1016/j.watres.2007.10.014, 2008.

Guo, S., Huang, H., Dong, X., and Zeng, S.: Calculation of greenhouse gas emissions of municipal wastewater treatment and its temporal and spatial trend in China, Water & Wastewater Engineering, 45, 56-62, https://doi.org/10.13789/j.cnki.wwe1964.2019.04.009, 2019.

Hase, F., Frey, M., Blumenstock, T., Groß, J., Kiel, M., Kohlhepp, R., Mengistu Tsidu, G., Schäfer, K., Sha, M. K., and Orphal, J.: Application of portable FTIR spectrometers for detecting greenhouse gas emissions of the major city Berlin, Atmos. Meas. Tech., 8, 3059-3068, https://doi.org/10.5194/amt-8-3059-2015, 2015.

Han, G., Pei, Z., Shi, T., Mao, H., Li, S., Mao, F., Ma, X., Zhang, X., and Gong, W.: Unveiling unprecedented methane hotspots in China's leading coal production hub: A satellite mapping revelation. Geophys. Res. Lett., 51, e2024GL109065, https://doi.org/10.1029/2024GL109065, 2024.

Heerah, S., Frausto-Vicencio, I., Jeong, S., Marklein, A. R., Ding, Y., Meyer, A. G., Parker, H. A., Fischer, M. L., Franklin, J. E., Hopkins, F. M., and Dubey, M.: Dairy methane emissions in California's San Joaquin Valley inferred with ground-based remote sensing observations in the summer and winter, J. Geophys. Res-Atmos., 126, e2021JD034785. https://doi.org/10.1029/2021JD03478, 2021.

Harada, T., and Alba, E.: Parallel Genetic Algorithms: A Useful Survey, ACM Comput. Surv., 53, 1-39, https://doi.org/10.1145/3400031, 2020.

He, Y., Li, Y., Li, X., Liu, Y., Wang, Y., Guo, H., Hou, J., Zhu, T., and Liu, Y.: Net-zero greenhouse gas emission from wastewater treatment: Mechanisms, opportunities and perspectives, Renew. Sust. Energ. Rev., 184, 113547, https://doi.org/10.1016/j.rser.2023.113547, 2023.

IPCC: Climate Change 2023: Synthesis Report. Contribution of Working Groups I, II and III to the Sixth Assessment Report of the Intergovernmental Panel on Climate Change, 35-115, https://doi.org/10.59327/IPCC/AR6-9789291691647, 2023.

683 Jackson, R. B., Down, A., Phillips, N. G., Ackley, R. C., Cook, C. W., Plata, D. L., and
684 Zhao, K.: Natural gas pipeline leaks across Washington, DC, Environ. Sci. Technol.,
685 48, 2051-2058, https://doi.org/10.1021/es404474x, 2014.
686 Jacob, D. J., Varon, D. J., Cusworth, D. H., Dennison, P. E., Frankenberg, C., Gautam,
687 R., Guanter, L., Kelley, J., McKeever, J., Ott, L. E., Poulter, B., Qu, Z., Thorpe, A.
688 K., Worden, J. R., and Duren, R. M.: Quantifying methane emissions from the global
689 scale down to point sources using satellite observations of atmospheric methane,
690 Atmos. Chem. Phys., 22, 9617–9646, https://doi.org/10.5194/acp-22-9617-2022,
691 2022.
692 Karion, A., Lauvaux, T., Lopez Coto, I., Sweeney, C., Mueller, K., Gourdji, S.,
693 Angevine, W., Barkley, Z., Deng, A., Andrews, A., Stein, A., and Whetstone, J.:
694 Intercomparison of atmospheric trace gas dispersion models: Barnett Shale case
695 study, Atmos. Chem. Phys., 19, 2561-2576, https://doi.org/10.5194/acp-19-2561-
696 2019, 2019.
697 Katoch, S., Chauhan, S.S. and Kumar, V.: A review on genetic algorithm: past, present,
698 and future. Multimed. Tools Appl., 80, 8091-8126, https://doi.org/10.1007/s11042-
699 020-10139-6, 2021.
700 Kissas, K., Ibrom, A., Kjeldsen, P., and Scheutz, C.: Methane emission dynamics from
701 a Danish landfill: The effect of changes in barometric pressure, Waste Manag., 138,
702 234-242, https://doi.org/10.1016/j.wasman.2021.11.043, 2022.
703 Kumar, P., Broquet, G., Yver-Kwok, C., Laurent, O., Gichuki, S., Caldow, C., Cropley,
704 F., Lauvaux, T., Ramonet, M., Berthe, G., Martin, F., Duclaux, O., Juery, C., Bouchet,
705 C., and Ciais, P.: Mobile atmospheric measurements and local-scale inverse
706 estimation of the location and rates of brief CH_4 and CO_2 releases from point sources,
707 Atmos. Meas. Tech., 14, 5987-6003, https://doi.org/10.5194/amt-14-5987-2021,
708 2021.
709 Li, H., You, L., Du, H., Yu, B., Lu, L., Zheng, B., Zhang, Q., He, K., and Ren, N.:
710 Methane and nitrous oxide emissions from municipal wastewater treatment plants in

China: A plant-level and technology-specific study, Environ. Sci. Technol., 20, 100345, https://doi.org/10.1016/j.ese.2023.100345, 2024.

Liang, R., Zhang, Y., Chen, W., Zhang, P., Liu, J., Chen, C., Mao, H., Shen, G., Qu, Z., Chen, Z., Zhou, M., Wang, P., Parker, R. J., Boesch, H., Lorente, A., Maasakkers, J.D., and Aben, I.: East Asian methane emissions inferred from high-resolution inversions of GOSAT and TROPOMI observations: a comparative and evaluative analysis, Atmos. Chem. Phys., 23, 8039-8057, https://doi.org/10.5194/acp-23-8039-2023, 2023.

Lin, X., Zhang, W., Crippa, M., Peng, S., Han, P., Zeng, N., Yu, L., and Wang, G.: A comparative study of anthropogenic CH_4 emissions over China based on the ensembles of bottom-up inventories, Earth Syst. Sci. Data, 13, 1073-1088, https://doi.org/10.5194/essd-13-1073-2021, 2021.

Lopez, M., Sherwood, O. A., Dlugokencky, E. J., Kessler, R., Giroux, L., and Worthy, D. E. J.: Isotopic signatures of anthropogenic CH_4 sources in Alberta, Canada, Atmos. Environ., 164, 280-288, https://doi.org/10.1016/j.atmosenv.2017.06.021, 2017.

Luther, A., Kleinschek, R., Scheidweiler, L., Defratyka, S., Stanisavljevic, M., Forstmaier, A., Dandocsi, A., Wolff, S., Dubravica, D., Wildmann, N., Kostinek, J., Jöckel, P., Nickl, A.-L., Klausner, T., Hase, F., Frey, M., Chen, J., Dietrich, F., Nęcki, J., Swolkień, J., Fix, A., Roiger, A., and Butz, A.: Quantifying CH_4 emissions from hard coal mines using mobile sun-viewing Fourier transform spectrometry, Atmos. Meas. Tech., 12, 5217-5230, https://doi.org/10.5194/amt-12-5217-2019, 2019.

Maazallahi, H., Fernandez, J. M., Menoud, M., Zavala-Araiza, D., Weller, Z. D., Schwietzke, S., von Fischer, J. C., Denier van der Gon, H., and Röckmann, T.: Methane mapping, emission quantification, and attribution in two European cities: Utrecht (NL) and Hamburg (DE), Atmos. Chem. Phys., 20, 14717-14740, https://doi.org/10.5194/acp-20-14717-2020, 2020.

Maazallahi, H., Delre, A., Scheutz, C., Fredenslund, A. M., Schwietzke, S., Denier van der Gon, H., and Röckmann, T.: Intercomparison of detection and quantification

methods for methane emissions from the natural gas distribution network in Hamburg, Germany, Atmos. Meas. Tech., 16, 5051-5073, https://doi.org/10.5194/amt-16-5051-2023, 2023.

Makarova, M. V., Alberti, C., Ionov, D. V., Hase, F., Foka, S. C., Blumenstock, T., Warneke, T., Virolainen, Y. A., Kostsov, V. S., Frey, M., Poberovskii, A. V., Timofeyev, Y. M., Paramonova, N. N., Volkova, K. A., Zaitsev, N. A., Biryukov, E. Y., Osipov, S. I., Makarov, B. K., Polyakov, A. V., Ivakhov, V. M., Imhasin, H. K., and Mikhailov, E. F.: Emission Monitoring Mobile Experiment (EMME): an overview and first results of the St. Petersburg megacity campaign 2019, Atmos. Meas. Tech., 14, 1047-1073, https://doi.org/10.5194/amt-14-1047-2021, 2021.

Masuda, S., Suzuki, S., Sano, I., Li, Y.-Y., and Nishimura, O.: The seasonal variation of emission of greenhouse gases from a full-scale sewage treatment plant, Chemosphere, 140, 167-173, https://doi.org/10.1016/j.chemosphere.2014.09.042, 2015.

Masuda, S., Sano, I., Hojo, T., Li, Y.-Y., and Nishimura, O.: The comparison of greenhouse gas emissions in sewage treatment plants with different treatment processes, Chemosphere, 193, 581-590, https://doi.org/10.1016/j.chemosphere.2017.11.018, 2017.

McKain, K., Down, A., Raciti, S. M., Budney, J., Hutyra, L. R., Floerchinger, C., Herndon, S. C., Nehrkorn, T., Zahniser, M. S., Jackson, R. B., Phillips, N., and Wofsy, S. C.: Methane emissions from natural gas infrastructure and use in the urban region of Boston, Massachusetts, Proc Natl Acad Sci USA, 112, 1941-1946, www.pnas.org/cgi/doi/10.1073/pnas.1416261112, 2015.

Mønster, J., Samuelsson, J., Kjeldsen, P., Rella, C.W., and Scheutz, C.: Quantifying methane emission from fugitive sources by combining tracer release and downwind measurements- A sensitivity analysis based on multiple field surveys, Waste Manag., 34:1416-1428, https://doi.org/10.1016/j.wasman.2014.03.025, 2014.

Moore, D. P., Li, N. P., Wendt, L. P., Castañeda, S. R., Falinski, M. M., Zhu, J.-J., Song, C., Ren, Z. J., and Zondlo, M. A.: Underestimation of sector-wide methane emissions

767 from united states wastewater treatment, Environ. Sci. Technol., 57, 4082-4090,
768 https://doi.org/10.1021/acs.est.2c05373, 2023.
769 Nassar, R., Hill, T. G., McLinden, C. A., Wunch, D., Jones, D. B. A., and Crisp, D.:
770 Quantifying CO_2 emissions from individual power plants from Space, Geophys. Res.
771 Let.t, 44, 10045-10053, https://doi.org/10.1002/2017GL074702, 2017.
772 Picarro: Datasheet G2201-i $\delta^{13}C$ in CH_4 and CO_2 Gas Analyzer, available at:
773 https://www.picarro.com/environmental/support/library/documents/g2201i_analyze
774 r_datasheet (last access: 5 August 2024), 2010.
775 Rees-White, T. C., Mønster, J., Beaven, R. P., and Scheutz, C.: Measuring methane
776 emissions from a UK landfill using the tracer dispersion method and the influence of
777 operational and environmental factors, Waste Manage., 87, 870-882, https://doi.
778 org/10.1016/j.wasman.2018.03.023, 2019.
779 Reinelt, T., Delre, A., Westerkamp, T., Holmgren, M.A., Liebetrau, J., and Scheutz, C.:
780 Comparative use of different emission measurement approaches to determine
781 methane emissions from a biogas plant. Waste Manag., 68, 173-185, http://dx.doi.
782 org/10.1016/j.wasman.2017.05.053, 2017.
783 Rella, C. W., Hoffnagle, J., He, Y., and Tajima, S.: Local- and regional-scale
784 measurements of CH_4, $\delta^{13}CH_4$, and C_2H_6 in the Uintah Basin using a mobile stable
785 isotope analyzer, Atmos. Meas. Tech., 8, 4539-4559, https://doi.org/10.5194/amt-8-
786 4539-2015, 2015.
787 Richardson, S. J., Miles, N. L., Davis, K. J., Lauvaux, T., Martins, D. K., Turnbull, J.
788 C., McKain, K., Sweeney, C., and Cambaliza, M. O. L.: Tower measurement network
789 of in-situ CO_2, CH_4, and CO in support of the Indianapolis FLUX (INFLUX)
790 Experiment. Elem. Sci. Anth., 5, 59, https://doi.org/10.1525/elementa.140, 2017.
791 Riddick, S. N., Connors, S., Robinson, A. D., Manning, A. J., Jones, P. S. D., Lowry,
792 D., Nisbet, E., Skelton, R. L., Allen, G., Pitt, J., and Harris, N. R. P.: Estimating the
793 size of a methane emission point source at different scales: from local to landscape,
794 Atmos. Chem. Phys., 17, 7839-7851, https://doi.org/10.5194/acp-17-7839-2017,

2017.

Scheutz, C., and Kjeldsen, P.: Guidelines for landfill gas emission monitoring using the tracer gas dispersion method. Waste Manage., 85, 351-360, https://doi.org/10.1016/j.wasman.2018.12.048, 2019.

Shi, T., Han, G., Ma, X., Mao, H., Chen, C., Han, Z., Pei, Z., Zhang, H., Li, S., and Gong, W.: Quantifying factory-scale CO_2/CH_4 emission based on mobile measurements and EMISSION-PARTITION model: cases in China, Environ. Res. Lett., 18, 034028, https://doi.org/10.1088/1748-9326/acbce7, 2023.

Song, C., Zhu, J.-J., Willis, J. L., Moore, D. P., Zondlo, M. A., and Ren, Z. J.: Methane emissions from municipal wastewater collection and treatment systems, Environ. Sci. Technol., 57, 2248-2261, https://doi.org/10.1021/acs.est.2c04388, 2023.

Stadler, C., Fusé, V. S., Linares, S., and Juliarena, P.: Estimation of methane emission from an urban wastewater treatment plant applying inverse Gaussian model, Environ. Monit. Assess., 194, 27, https://doi.org/10.1007/s10661-021-09660-4, 2021.

Sun, W., Deng, L., Wu, G., Wu, L., Han, P., Miao, Y., and Yao, B.: Atmospheric monitoring of methane in Beijing using a mobile observatory, Atmosphere, 10, 554, https://doi.org/10.3390/atmos10090554, 2019.

Sun, Y., Yang, T., Gui, H., Li, X., Wang, W., Duan, J., Mao, S., Yin, H., Zhou, B., Lang, J., Zhou, H., Liu, C., and Xie, P.: Atmospheric environment monitoring technology and equipment in China: A review and outlook, J. Environ. Sci., 123, 41-53, https://doi.org/10.1016/j.jes.2022.01.014, 2023.

Venkatram, A. and Horst, T. W.: Approximating dispersion from a finite line source, Atmos. Environ., 40, 2401-2408, https://doi.org/10.1016/j.atmosenv.2005.12.014, 2006.

Vítěz, T., Novák, D., Lochman, J., and Vítězová, M.: Methanogens diversity during anaerobic sewage sludge stabilization and the effect of temperature, Processes, 8, 822, https://doi.org/10.3390/pr8070822, 2020.

Vogel, F., Ars, S., Wunch, D., Lavoie, J., Gillespie, L., Maazallahi, H., Röckmann, T.,

Nęcki, J., Bartyzel, J., Jagoda, P., Lowry, D., France, J., Fernandez, J., Bakkaloglu, S., Fisher, R., Lanoiselle, M., Chen, H., Oudshoorn, M., Yver-Kwok, C., Defratyka, S., Morgui, J. A., Estruch, C., Curcoll, R., Grossi, C., Chen, J., Dietrich, F., Forstmaier, A., Denier van der Gon, H. A. C., Dellaert, S. N. C., Salo, J., Corbu, M., Iancu, S. S., Tudor, A. S., Scarlat, A. I., and Calcan, A.: Ground-based mobile measurements to track urban methane emissions from natural gas in 12 cities across eight countries, Environ. Sci. Technol., 58, 2271-2281, https://doi.org/10.1021/acs.est.3c03160, 2024.

von Fischer, J. C., Cooley, D., Chamberlain, S., Gaylord, A., Griebenow, C. J., Hamburg, S. P., Salo, J., Schumacher, R., Theobald, D., and Ham, J.: Rapid, Vehicle-based identification of location and magnitude of urban natural gas pipeline leaks, Environ. Sci. Technol., 51, 4091-4099, https://doi.org/10.1021/acs.est.6b06095, 2017.

Wang, X., Wang, T., Chen, S., and Tang, Y.: Study on methane emission from wastewater treatment plants-A case study of Wuhu city, Advances in Geosciences, 11, 677-689, https://doi.org/10.12677/AG.2021.115063, 2021.

WMO：WMO greenhouse gas Bulletin. The state of greenhouse gases in the atmosphere based on global observations through 2022. https://library.wmo.int/idurl/4/68532, 2023.

Weller, Z. D., Roscioli, J. R., Daube, W. C., Lamb, B. K., Ferrara, T. W., Brewer, P. E., and von Fischer, J. C.: Vehicle-based methane surveys for finding natural gas leaks and estimating their size: Validation and uncertainty, Environ. Sci. Technol., 52, 11922-11930, https://doi.org/10.1021/acs.est.8b03135, 2018.

Weller, Z. D., Yang, D.K., von Fischer, J.C.: An open source algorithm to detect natural gas leaks from mobile methane survey data, PLoS ONE, 14, e0212287, https://doi.org/10.1371/journal.pone.0212287, 2019.

Yacovitch, T. I., Herndon, S. C., Petron, G., Kofler, J., Lyon, D., Zahniser, M. S., and Kolb, C. E.: Mobile laboratory observations of methane emissions in the Barnett Shale Region, Environ. Sci. Technol., 49, 7889-7895, https://doi.org/10.1021/

es506352j, 2015.

Yin, Y., Qi, X., Gao, L., Lu, X., Yang, X., Xiao, K., Liu, Y., Qiu, Y., Huang, X and Liang, P.: Quantifying methane influx from sewer into wastewater treatment processes, Environ. Sci. Technol., 58, 9582-9590, https://doi.org/10.1021/acs.est.4c00820, 2024.

Yoshida, H., Mønster, J., and Scheutz, C.: Plant-integrated measurement of greenhouse gas emissions from a municipal wastewater treatment plant, Water Res., 61, 108-118, http://dx.doi.org/10.1016/j.watres.2014.05.014, 2014.

Zhang, Y., Jacob, D. J., Lu, X., Maasakkers, J. D., Scarpelli, T. R., Sheng, J.-X., Shen, L., Qu, Z., Sulprizio, M. P., Chang, J., Bloom, A. A., Ma, S., Worden, J., Parker, R. J., and Boesch, H.: Attribution of the accelerating increase in atmospheric methane during 2010-2018 by inverse analysis of GOSAT observations, Atmos. Chem. Phys., 21, 3643-3666, https://doi.org/10.5194/acp-21-3643-2021, 2021.

Zhao, S., Zhang, Y., Liang, R., Chen, W., Xie, X., Wang, R., Xia, Z., Shen, J., Wang, Y., and Chen, H.: Low methane emissions from the natural gas distribution system indicated by mobile measurements in a Chinese megacity Hangzhou, Environ. Sci. Technol. Air, 1, 1511-1518, https://doi.org/10.1021/acsestair.4c00068, 2024.

Zhao, T., Yang, D., Liu, Y., Cai, Z., Yao, L., Che, K., Ren, X., Bi, Y., Yi, Y., Wang, J., and Zhu, S.: Development of an integrated lightweight multi-rotor UAV payload for atmospheric carbon dioxide mole fraction measurements, Atmosphere, 13, 855, https://doi.org/10.3390/atmos13060855, 2022.

Zhao, Y., Xue, M., Li, X., Liu, G., Liu, S., and Sun, X.: Application of vehicle-mounted methane detection method in the oil and gas industry, Environmental Protection of Oil & Gas Fields, 31, 4, https://doi.org/10.3969/j.issn.1005-3158.2021.04.001, 2021.

Zimnoch, M., Necki, J., Chmura, L., Jasek, A., Jelen, D., Galkowski, M., Kuc, T., Gorczyca, Z., Bartyzel, J., and Rozanski, K.: Quantification of carbon dioxide and methane emissions in urban areas: source apportionment based on atmospheric observations, Mitig. Adapt. Strateg. Glob. Change, 24, 1051-1071, https://doi.org/

879 10.1007/s11027-018-9821-0, 2018.